Surface Science 674 (2018) 103–114

Contents lists available at ScienceDirect

Surface Science

journal homepage: www.elsevier.com/locate/susc

Half-metallic property of the bulk and (001) surfaces of MNaCs (M = P, As) half-Heusler alloys: A density functional theory approach

Mohammad Rostami[a,b,*]

[a] Faculty of Physics, Kharazmi University, Tehran, Iran
[b] Applied Science Research Center, Kharazmi University, Karaj, Iran

ARTICLE INFO

Keywords:
Half-Heusler alloys
Surface properties
Density functional theory
Half-metallic ferromagnets
Magnetic properties

ABSTRACT

The structural, electronic and half-metallic properties of bulk and (001) surfaces of MNaCs (M = P, As) half-Heusler alloys are investigated. The half-metallic property have been observed in both of these materials. The spin-flip gaps of PNaCs and AsNaCs are found to be 0.25 and 0.21 eV, and the Curie temperatures are estimated to be 478.24 and 474.07 K within the mean field approximation, respectively. The mechanisms of half-metallicity in these materials are studied by considering the spin-dependent band structures and the atomic density of states. The preservation of the half-metallic ferromagnetism under stress are also investigated. The symmetric slab model is employed for the investigation of the (001) surfaces of the compounds because the electron spin polarization at the bulk of the materials does not guarantee the spin-polarization at the surfaces of them. It turns out that the half-metallic ferromagnetism is well preserved for P (As)-terminated surfaces, but it is removed at the NaCs-terminated surfaces of both of the compounds.

1. Introduction

The researches on the role played by the spin of the electrons in solid state devices for various applications such as memory storage and read heads are referred to spintronic [1–4]. Spintronic have attracted much research interests and it has made significant contributions to the advances in information technology [5–7]. One of the crucial purposes and challenges in spintronic devices is the production of spin-polarized currents [8–10]. The application of half-metals in spintronic devices is known to be a promising way to produce spin-polarized currents [11,12]. These kinds of the materials have dissimilar electronic properties for spin-up and spin-down states such that they show metallic behavior for one of the spin states, and semiconducting behavior for the other [13].

Half-metallic ferromagnetism have been distinguished in some kinds of the materials. The binary compounds such as MoTe and MnBi in zinc-blende structure, KM (M = P, Se and Te) in rocksalt and zinc-blende structure, TiTe in wurtzite structure [14–19], half-metallic oxides such as Sr_2CrWO_6 thin films, AMnO3 (A = Mg, Ca) and $XFeO_3$ (X = Sr, Ba) [20–22], 2D materials such as V_{Ge}@Fe and Co and V_C@*Sc*, Fe and Co in two-dimensional GeC with single vacancy, monolayer honeycomb structures of group-V binary compounds and C_2N-h2D nanoribbons doped with Ni [23–26], full Heusler alloys such as ZrRhTiIn, ZrCrCoZ (Z = B, Al, Ga, In), $NaTO_2$ (T = *Sc*, Ti, V, Cr, and Mn), MCoTiZ (M = Lu, La; Z = Si, Ge, Sn), ScCoTiN (N = Si, Ge), RbCaNZ (Z = O, S, and Se) and MnY_2Z (Z = Al, Si, Ga, Ge, Sn, Sb) [27–32], and half-Heusler compounds such as CoCrBi, XYZ (X = Ni; Y = Cr; Z = Si, Ge, Ga, Al, In, As), RuMnZ (Z = P, As) and YZSb (Z = Cr, Mn) [33-36], and doped materials such as $Zn_{0.75}Mo_{0.25}Te$, Cr-doped MC (M = Si, Ge and Sn), Mn doped (ZnO:Mn) and (Mn,Cr) co-doped zinc oxide (ZnO:(Mn,Cr)), C-doped at S-site in BeS, and Ga and Zn-doped CrP are some of the materials that are predicted to be half-metals [14,37–40].

Among these kinds of the materials, the compounds with no transition elements (d^0-compounds) seem to be more appropriate than the others because of their rather high Curie temperatures [41]. Besides, the presence of transition elements in these compounds causes a large magnetic moment in the material which leads to the stray of the magnetic fields that result in great amount of energy loss in spintronic devices [42]. Heusler alloys also attract many research interests due to their rather high Curie temperatures and their almost similar crystal structure to the semiconductors, and as a result, they could be grown over the semiconductor substrates. For example, Co_2MnSi films were grown on As-terminated GaAs (100) by molecular beam epitaxy using different first atomic layers: MnSi, Co, and Mn [43]. Half-Heusler Co-$Ti_{1-x}Fe_xSb$ were grown by molecular beam epitaxy on InAlAs/InP(001) substrates for concentrations $0.0 \leq x \leq 1.0$, and $Co_2FeAl_{0.5}Si_{0.5}$ was also grown over Si (111) and Ge (111) substrates [44–46].

Therefore, it is so advantageous to find half-metallic Heusler alloys

* Corresponding author at: Faculty of Physics, Kharazmi University, Tehran, Iran.
E-mail address: mrostami@khu.ac.ir.

https://doi.org/10.1016/j.susc.2018.04.006
Received 17 January 2018; Received in revised form 28 March 2018; Accepted 10 April 2018
Available online 13 April 2018
0039-6028/

Table 1
The positions of the atoms in three possible atomic arrangements for MNaCs (M = P, As) half-Heusler alloys.

Compound	M	Na	Cs
Type a	(0 0 0)	(0.25 0.25 0.25)	(0.75 0.75 0.75)
Type b	(0.25 0.25 0.25)	(0 0 0)	(0.75 0.75 0.75)
Type c	(0 0 0)	(0.5 0.5 0.5)	(0.75 0.75 0.75)

without transition elements as potential materials in spintronic devices because they could have low magnetic moments, high Curie temperatures and similar crystal structures to the semiconductors. Here, PNaCs and AsNaCs half-Heusler alloys have been considered, and the results of our calculations show that both of these compounds are half-metallic ferromagnets with the low magnetic moment of 1 μ_B and the Curie temperatures of 478.24 and 474.07 K, respectively.

From the practical point of view, it is so important to consider the surface properties of the half-metals. Actually, an efficient half-metallic ferromagnet should preserve the half-metallicity at its surfaces to transfer the spin-polarized current to the other parts of the spintronic instruments. For example, the half-metallicity of bulk MnBi is preserved on the (001), (110) and (111) surfaces except for the Bi-terminated (001) and Mn-terminated (111) surfaces [15]. The SnSn termination have the highest spin polarizations P = 77.1% among the other Zr_2CoSn (001) surfaces [47]. Co_2CrAl/GaAs (111) surface shows 80% spin polarization, and the spin polarization has enhanced using capping layers of Au and Cu [48]. Co–Co/V–Al and Co–Mn/Mn–Al interfaces preserve the half-metallic character at the Co_2MnAl/CoMnVAl heterostructure [49]. The half-metallic property of the bulk Ti_2FeSn are retained at the TiSn and TiFe terminated (001) surfaces, however the FeFe*, TiTi* and SnSn* terminations does not preserve the bulk half-metallicity [50]. The (111) surfaces of FeCrSe with Cr and Fe terminations lose the bulk half-metallicity, but Se-terminated (111) and (001) surface with CrSe termination preserve the bulk half-metallic property [51]. The half-metallicity is destroyed on the Fe–Cr, Nb–Al, Fe–V, and Nb–Ge terminated (001) surfaces of NbFeCrAl and NbFeVGe quaternary Heusler compounds [52].

Until now, there are few studies on surface properties of d^0 Heusler alloys. Therefore, in this article, the electronic and half-metallic properties of the M-terminated and NaCs-terminated (001) surfaces of MNaCs (M = P, As) are also considered. The results of our calculations show that half-metallic ferromagnetism is well preserved for P (As)-terminated surfaces, but it is removed at the NaCs-terminated surfaces for both of the compounds. Considering the appropriate properties of the bulk and surfaces of MNaCs (M = P, As), it seems that PNaCs and AsNaCs are potential candidates in spintronic applications.

2. Computational details

Density functional theory with GGA approximation was employed to obtain the structural, electronic and half-metallic properties of the bulk and surfaces of the samples [53,54]. Quantum-ESPRESSO simulation package was used to solve Kohn–Sham equations with plane wave basis sets [55]. Kinetic energy cutoffs of 35Ry and 350Ry were

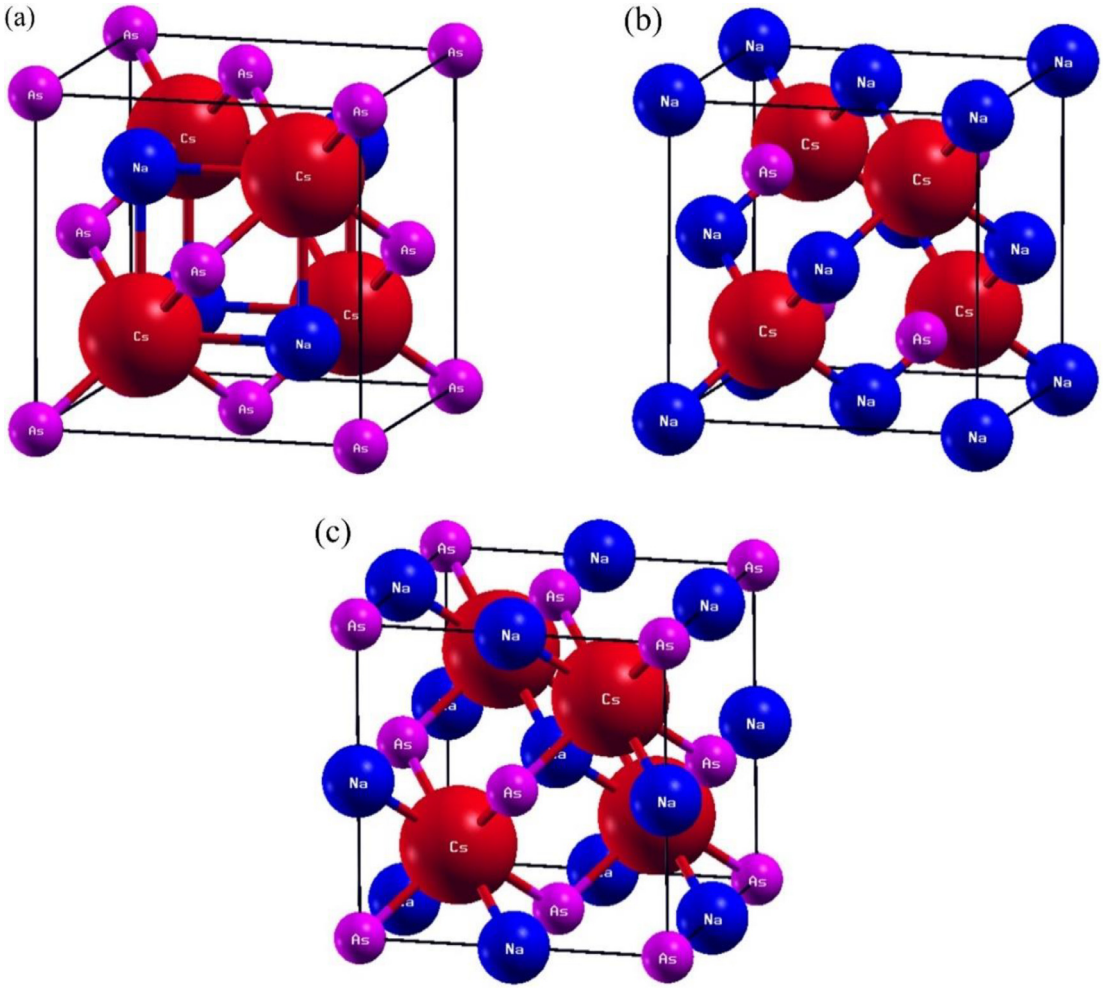

Fig. 1. Crystal structures of three different types of AsNaCs half-Heusler alloy for (a) type *a*, (b) type *b*, and (c) type *c*.

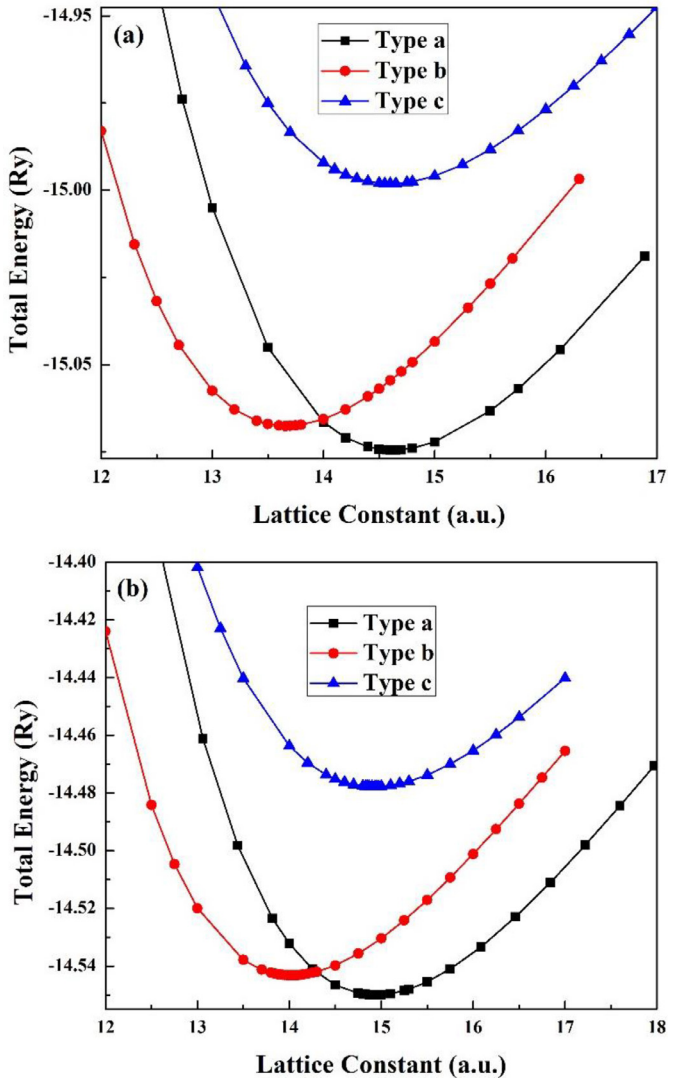

Fig. 2. Total energy versus lattice constant for (a) PNaCs and (b) AsNaCs in three types of half-Heusler alloys.

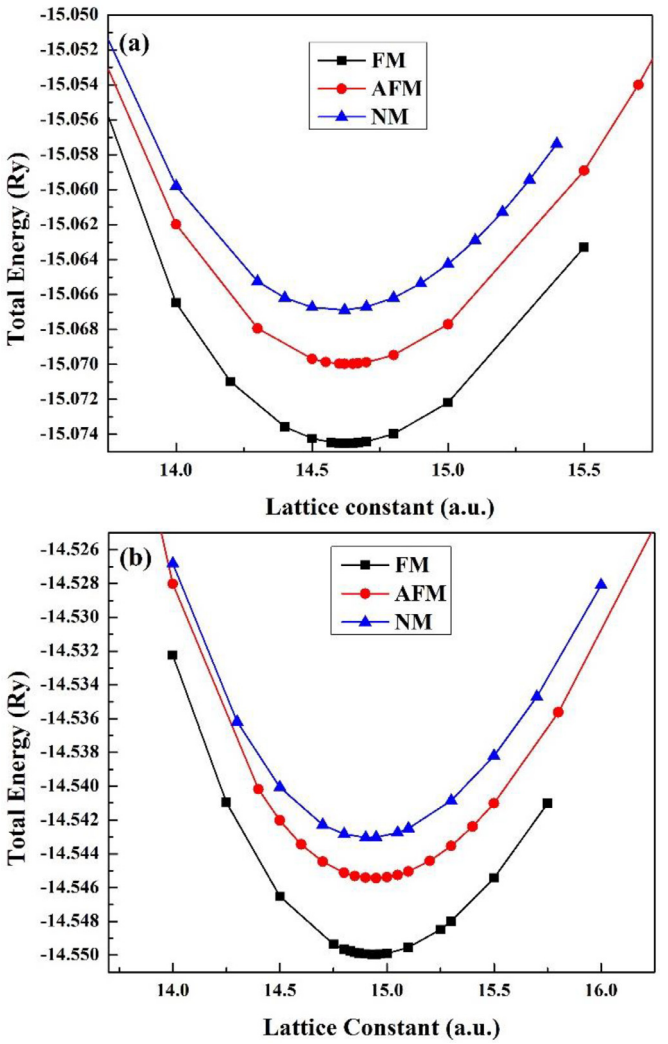

Fig. 3. Total energy versus lattice constant for (a) PNaCs and (b) AsNaCs in FM, AFM and NM phases.

used for wave function and charge density expansions, respectively. The integrations were carried out utilizing Monkhorst-Pack grids of $10 \times 10 \times 10$ and $12 \times 12 \times 1$ K-points for the bulk and surfaces, respectively [56]. The convergence thresholds for self-consistency were 10^{-5} and 10^{-4} a.u. for total energy and force, respectively.

3. Results and discussion

3.1. Bulk properties

3.1.1. Structural properties

The half-Heusler alloys with the space group of $F\bar{4}3m$ could be considered as the sublattices of the zinc-blende structure where the octahedral places are occupied. The general formula of these compounds is shown by XYZ, and the crystal structure of them is constructed by three interpenetrating FCC lattices. Each of the X, Y and Z atoms are situated at one of the FCC lattices, and it could be shown by the symmetry reasons that there are three possible arrangements for the half-Heusler alloys named types *a, b* and *c*. The coordinates of the atoms in three possible atomic arrangements for MNaCs (M = P, As) half-Heusler alloys are listed in Table 1, and Fig. 1 represents these three types for AsNaCs.

First, we have calculated the total energies in three types of half-Heusler alloys for MNaCs (M = P, As). The results of our calculations are represented in Fig. 2, and it seems that type *a* is the most stable crystal structure for both PNaCs and AsNaCs. It is also found from Fig. 3 that these materials in ferromagnetic (FM) phase are more stable than nonmagnetic (NM) and antiferromagnetic (AFM) phases (see Fig. 3). The equilibrium lattice constants for type *a* in FM phase as well as the bulk modulus of the compounds are also found by fitting the total energy as a function of volume to the Murnaghan equation of state, and the corresponding results are represented in Table 2.

3.1.2. Electronic and magnetic properties

The density of states diagrams of the samples are illustrated in Fig. 4. We can see from this figure that the Fermi energy is in gap for majority spin states, and in the conduction band for minority spin states for both of these compounds, and as a result, they have half-metallic property and could produce 100% spin-polarized currents. The spin-flip gaps of PNaCs and AsNaCs which are equal to the difference between the Fermi level and the highest energy of the spin-up conduction band are listed in Table 2. The calculated total and atomic magnetic moments are listed in Table 3. It seems that most of the magnetic moment originate from P atoms of PNaCs and As atoms of AsNaCs.

Next, it is important to find the origin of half-metallic ferromagnetism by considering the partial density of states and the band structures for both of the spin states. We just represent the atomic

Table 2
The lattice constant, bulk modulus, Spin-flip gap and Curie temperature of PNaCs and AsNaCs.

Compound	Lattice constant(A°)	Bulk modulus (GPa)	Spin-flip gap (eV)	Curie temperature (K)
PNaCs	7.74	16.0	0.25	478.24
AsNaCs	7.91	12.5	0.21	474.07

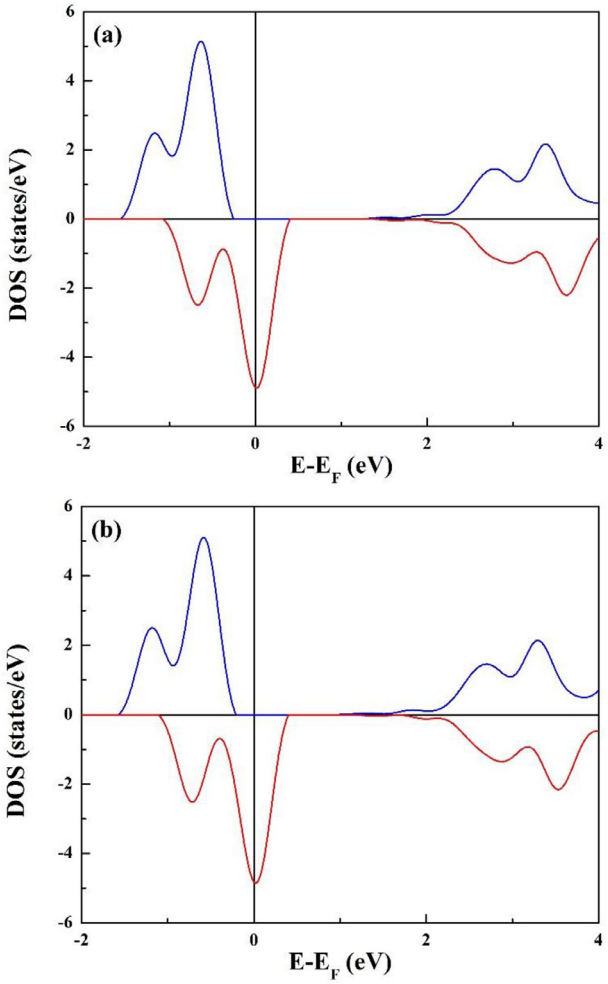

Fig. 4. The total density of states (DOS) diagrams for (a) PNaCs and (b) AsNaCs.

Table 3
The atomic and total magnetic moment in Bohr magneton (μ_B) on each atom for MNaCs (M = P and As) compounds.

Compound	Na	Cs	M	Total
PNaCs	−0.0046	0.0453	0.9682	1.0089
AsNaCs	0.0081	0.0610	0.9501	1.0192

density of the states for PNaCs because of the same mechanisms in these compounds (see Fig. 5). Figs. 6 and 7 also show the band structure diagrams for PNaCs and AsNaCs, respectively. The origin of half-metallicity in d^0 compounds are not similar to the half-Heusler alloys with transition metals. In half-Heusler alloys with transition elements, the bonding-antibonding splitting and the gap between them is achieved as a result of the hybridization of p orbital of main-group element and t_{2g} orbital of the transition metal. As a result of the exchange splitting, the gap between the bonding and anti-bonding states is located at different energies for majority and minority spin states, and the Fermi energy is

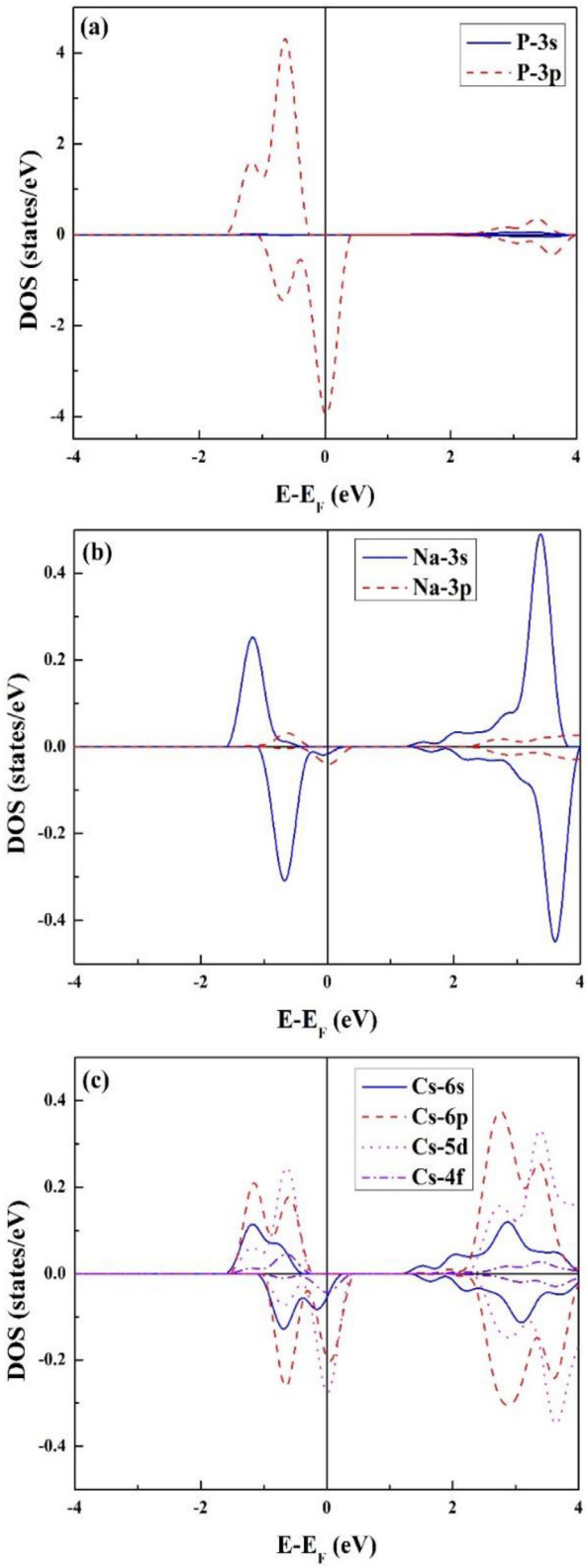

Fig. 5. The partial density of states for PNaCs at the equilibrium lattice constant.

in gap for one of the spin-states which leads to half-metallicity in these kinds of the materials [57].

Comparing Figs. 5 and 6, it becomes clear that the observed bands in the vicinity of the Fermi level are originated from P-p orbitals. The presence of the molecular field causes the bands to have different

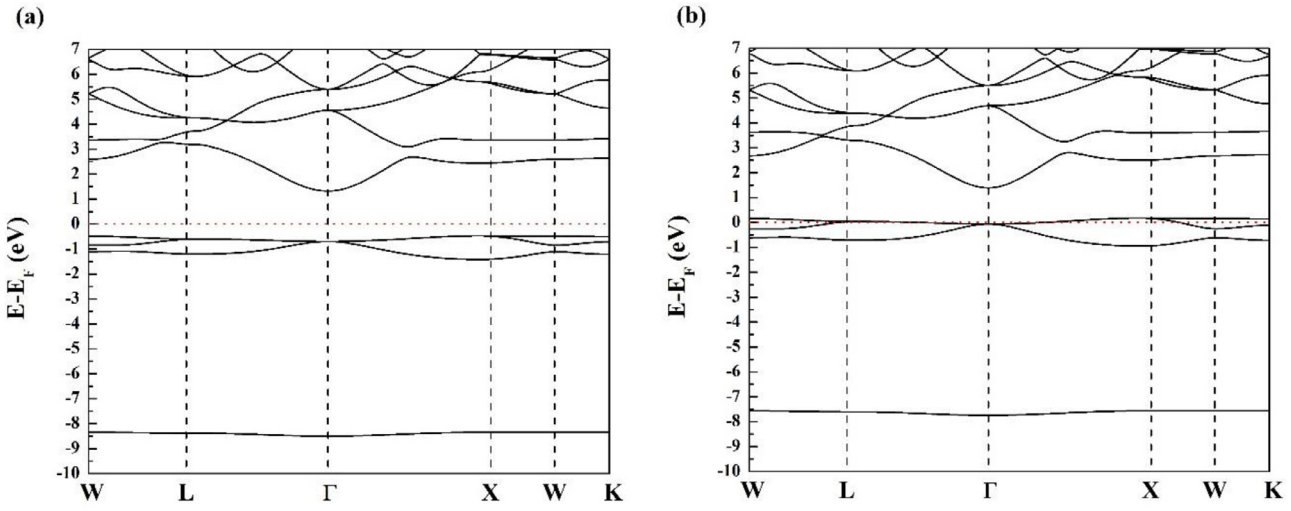

Fig. 6. The band structures of PNaCa for (a) majority, and (b) minority spin states.

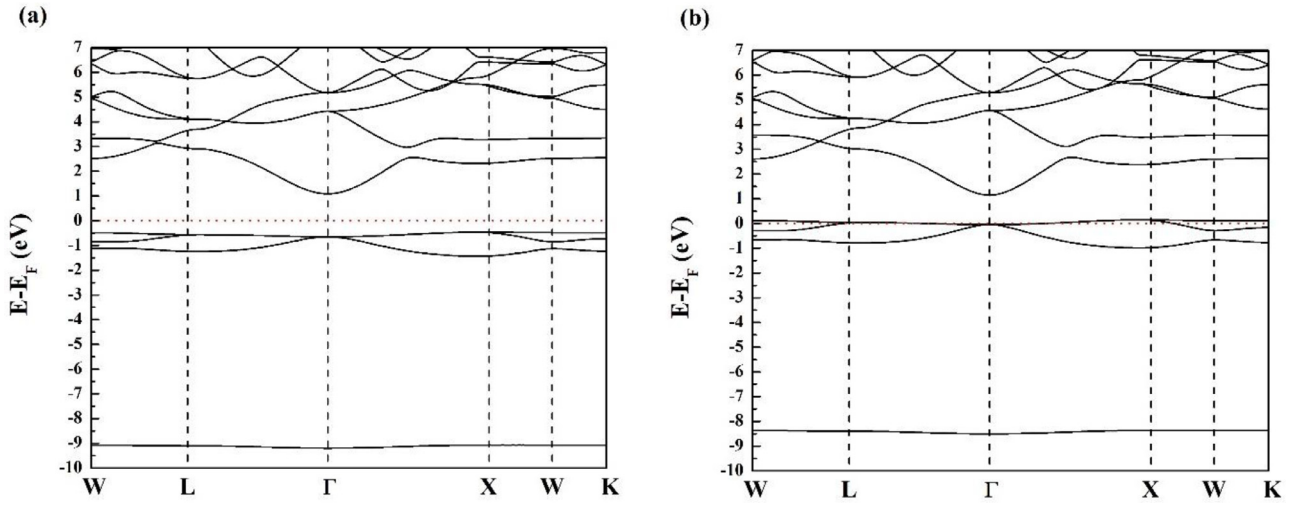

Fig. 7. The band structures of AsNaCa for (a) majority, and (b) minority spin states.

energies relative to the Fermi energy. An electron with the same spin-direction as the magnetic field has lower energy than the one with the opposite spin-direction. Since the energy difference is greater than the band width originated from P–p orbitals, the samples have the half-metallic property because of the presence of the Fermi level in just spin-up states.

The half-metallic ferromagnetism of the compounds under stress should also be considered because most of the half-metals are grown over the semiconductors for spintronic applications [58–60], and the lattice mismatches between the half-metal and the semiconductor can cause stress on the half-metal [60–62]. This stress can change the lattice constant and the band structure of the material in such a way that the half-metallic property could be lost. Fig. 8 shows the valance band maximum and conduction band minimum energy relative to Fermi level in majority spin states for PNaCs and AsNaCs at different lattice constants. In cases where the Fermi surface touches the valence band maximum or conduction band minimum in spin-up states, the half-metallicity would be removed. We can see from these figures that for both of the compounds, the Fermi energy approaches the lowest energy of the conduction at the lattice constants higher than the equilibrium lattice constant, and the valance band maximum for the lattice constants smaller than the equilibrium lattice constant. Considering Fig. 8, it seems that the half-metallic property is well conserved for lattice compressions from −9.8% to +31.1%, and from −9.9% to +31.5% for PNaCs and AsNaCs, respectively. Therefore, these materials are appropriate candidates to be grown over the semiconductors for spintronic applications.

An appropriate half-metallic ferromagnet should also maintain its property at temperatures as high as room temperature. The Curie temperatures of the samples have been estimated in the mean field approximation. According to this approximation, the Curie temperature could be evaluated with the following equation:

$$T_C = \frac{2\Delta E}{3k_B} \tag{1}$$

where ΔE is the energy difference between the ferromagnetic and antiferromagnetic states. The results of our calculations are listed in Table 2 which shows that these temperatures are well above room temperature.

3.2. Surface analysis

Symmetric slabs including two identical surfaces are employed for exploring the electronic and half-metallic properties of the (001) surfaces of MNaCs (M = P, As). A layer of vacuum is used to prevent the blades from interacting. The thickness of the slabs should be optimized such that the atoms with the same electronic and magnetic properties as the bulk should be observed at the central layers of the slab. Here, we

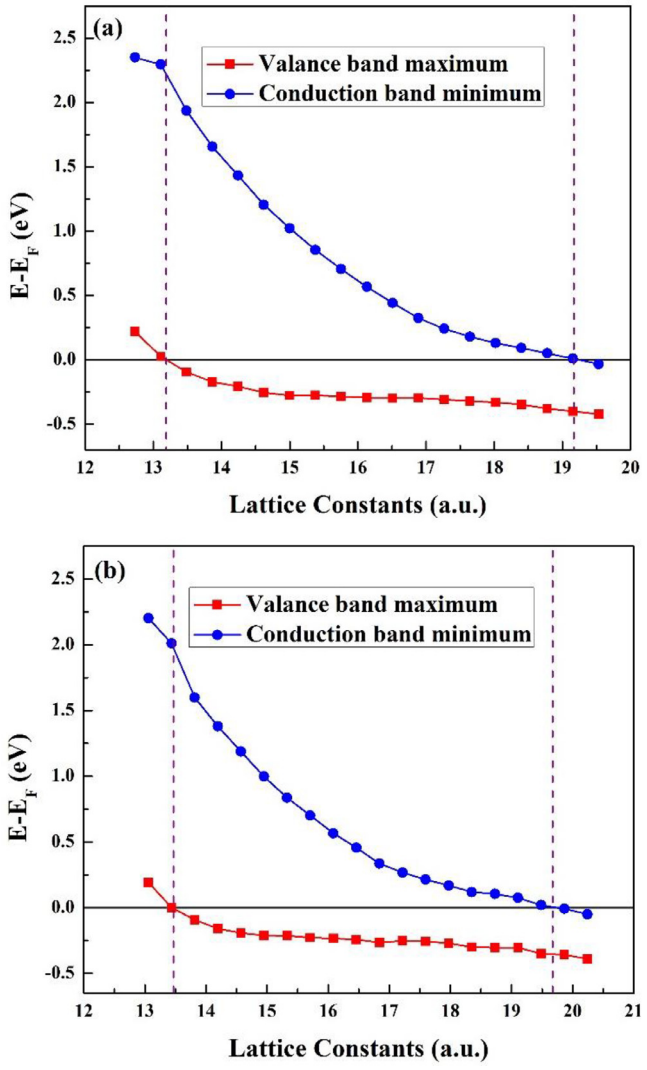

Fig. 8. The valance band maximum and conduction band minimum energy relative to Fermi energy in majority spin states for (a) PNaCs, and (b) AsNaCs at different lattice constants.

conclude that a slab with eleven atomic layers, and a vacuum width of 20 a.u. are appropriate for the simulation of the (001) surfaces.

According to Fig. 1a, there are two kinds of (001) surfaces for MNaCs (M = P and Cs) half-Heusler compounds with type α crystal structure that are the surface including P (As) atoms and the one including both of Na and Cs atoms. Therefore, two kinds of slabs are used to simulate (001) surfaces which are P (As)-terminated and NaCs-terminated slabs. Fig. 9 shows these two type of slabs for AsNaCs. The atomic positions have been relaxed along the surface normal expect for the atoms at the three central layers of the slab that were kept motionless at the bulk places. The atomic positions in the P (As)-terminated and NaCs-terminated slabs before and after relaxations have been tabulated in the supplementary material (see supplementary Tables SI to SVIII).

After the relaxation of atomic positions, the surface atoms at the P (As)-terminated slabs tend to approach inside the slab, whereas the subsurface Na atoms move outside the slab and subsurface Cs atoms move slightly inward the slab. The surface Cs atoms and the subsurface P (As) atoms at the NaCs-terminated slabs approach slightly toward the vaccum, but the surface Na atoms go toward slab. As a result of these changes in the atomic positions, the P (As)–Na bond length decreases by

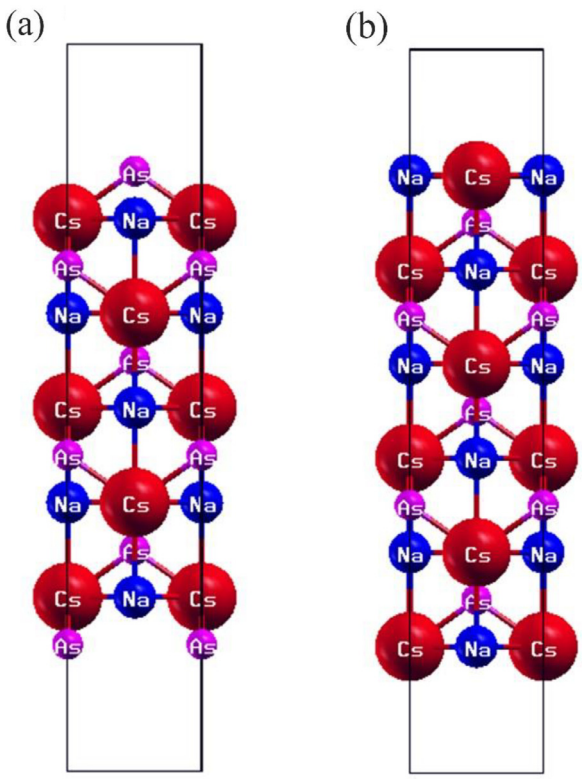

Fig. 9. (a) As-terminated (001), (b) NaCs-terminated (001) slabs of AsNaCs.

$0.51A^o(0.50A^o)$ at the NaCs-terminated slab, while P (As)-Cs and Na-Cs bond lengths increase by $0.03A^o(0.02A^o)$ and $0.18A^o(0.17A^o)$ respectively. The P (As)-Na and P (As)–Cs bond lengths decrease by $0.49A^o(0.47A^o)$ and $0.08A^o(0.06A^o)$ at the P (As)-terminated slab, respectively; however, Na-Cs bond length increases by $0.11A^o(0.11A^o)$.

Therefore, it seems that the relaxation affect the atomic positions at the NaCs-terminated slab more than P (As)-terminated one. Among the atoms, the changes in the Na position at the NaCs-terminated slab were more than the others because four P nearest neighbors have been missed from the surface Na atoms and the electrons at the broken bonds were relocated to the subsurface P (As) ions due to the greater electronegativity of P (As) than Na atoms. A partial positive charge on the surface Na ions and partial negative charge on P (As) and the smaller atomic mass of Na than Cs atoms cause the Na ions to move toward the slab. The movement of the subsurface Na ion at the P (As)-terminated slab as a result of the relaxation is also more than the other ions. Actually, the existence of the electrons on the broken bonds cause surface P ions to have more partial negative charge than the other P ions, and as a result, Na ions with partial positive charge tend to move outside the slab (vacuum).

Density of states for the atoms at various positions of the NaCs-terminated and P-terminated slabs of PNaCs are given in Figs. 10 and 11. The same diagrams for NaCs-terminated and As-terminated (001) slabs of AsNaCs are also given in Figs. 12 and 13, respectively. The location-dependent atomic magnetic moments for the (001) slabs of PNaCs and AsNaCs have been shown in Tables 4 and 5, respectively.

According to Figs. 10–13 and Tables 4 and 5, we find that the slabs with appropriate thicknesses was chosen for considering the electronic and half-metallic properties of the surfaces because we could see almost the same DOS diagram and magnetic moment values for the atoms at the central layer and the bulk. We can see from these figures that the half-metallicity is removed at the NaCs-terminated surfaces of both PNaCs and AsNaCs compounds. However, the half-metallicity is well

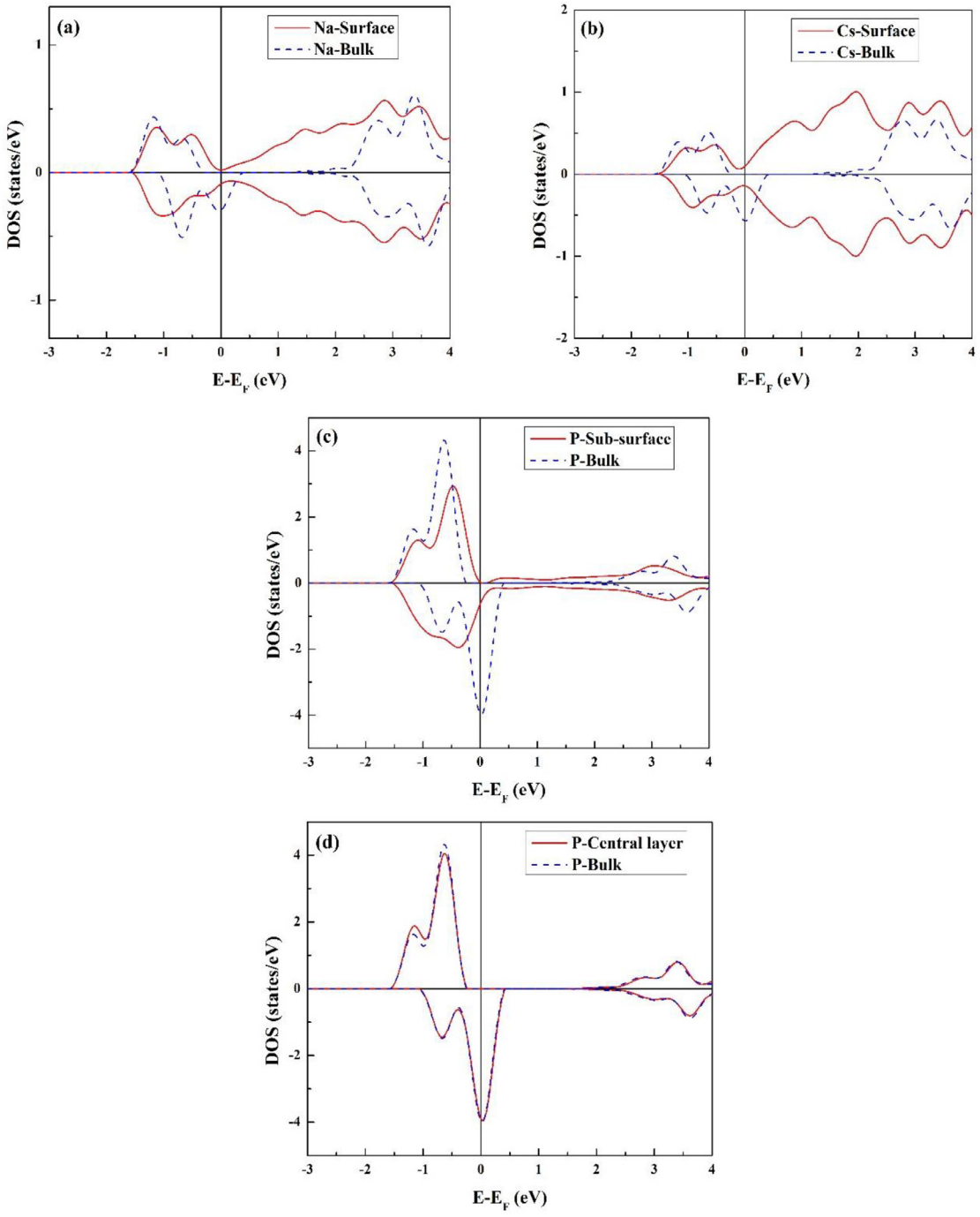

Fig. 10. The atomic density of states at various positions of the NaCs-terminated (001) slab of PNaCs. The corresponding diagram for the bulk atoms are also given for analyzing.

preserved for P-terminated and As-terminated (001) surfaces of PNaCs and AsNaCs, respectively. Therefore, it seems that MNaCs (M = P, As) half-Heusler compounds with the P (As)-terminated (001) surfaces are appropriate materials to grow them on semiconductors for various spintronic applications.

We can see from Tables 3 and 4 that the polarization of the surface Na and Cs and subsurface P (As) for NaCs-terminated suface of PNaCs (AsNaCs) decreases with respect to the bulk values. These changes are related to the decrease in the spin-splitting of the samples that are caused by the shift of the spin-up states toward higher energies with respect to the bulk. Especially for the subsurface P (As) atoms, the magnetic moment decreases by about 90.2% (91.0%) which is due to the large decrease in the spin-splitting compared to the bulk (see Fig. 10c and 12c).

However, the magnetic moments of the exterior atoms at the P (As)-terminated slabs are grown relative to the bulk which are related to an increase in the spin-splitting. The polarization of the surface P (As) ions increases by about 68.7% (71.5%) that is caused by the shift of the spin-up states toward lower energies. For the subsurface Na and Cs atoms, we could see the shift of both spin-up and spin-down states toward

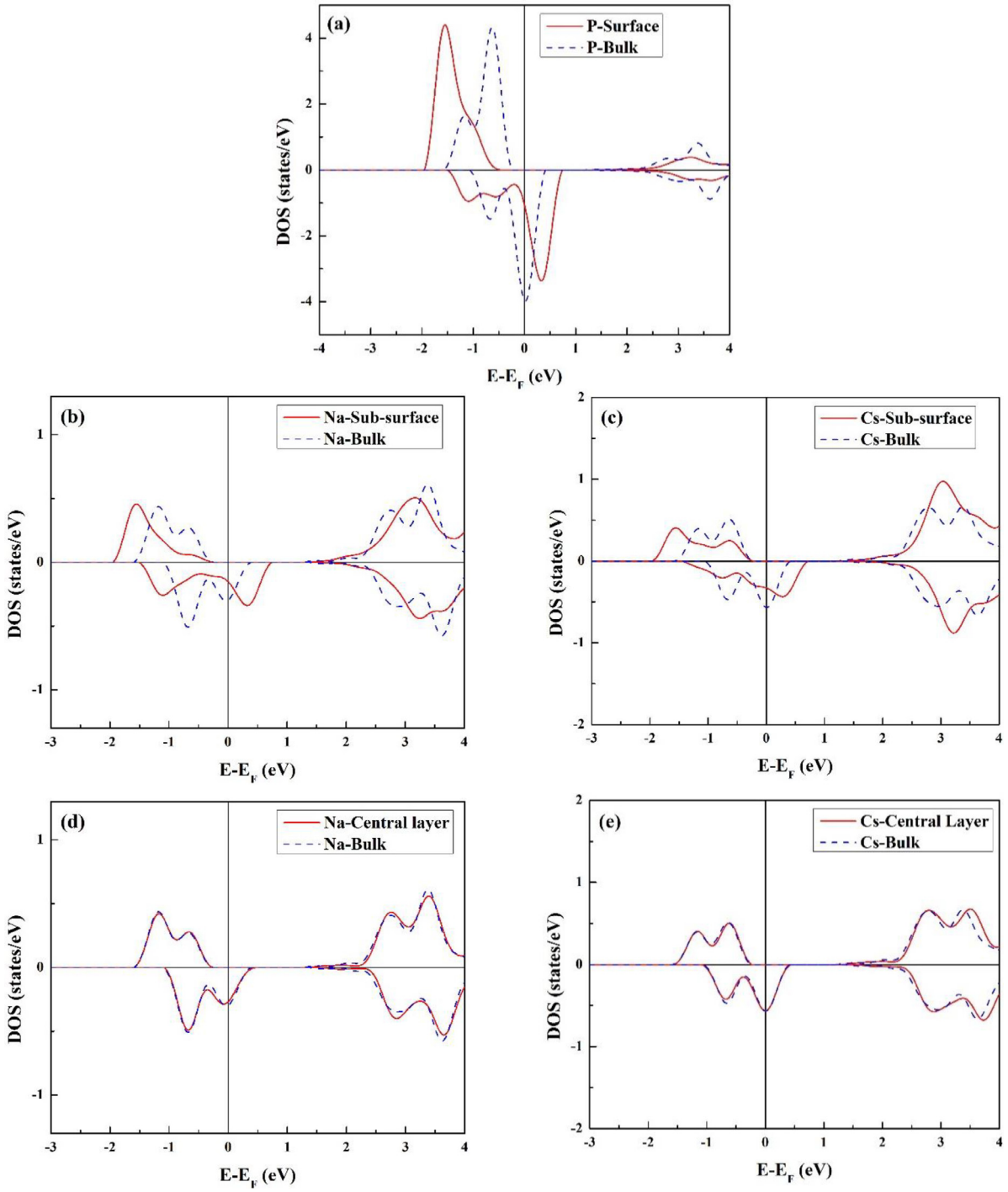

Fig. 11. The atomic density of states at various positions of the P-terminated (001) slab of PNaCs. The corresponding diagram for the bulk atoms are also given for analyzing.

lower energies, and therefore smaller changes in the values of the magnetic moments are observed for these atoms than surface P (As) atoms.

Most of the changes and surface effects mentioned above stem from disconnected chemical bonds and relaxation of the atomic positions at the surfaces. Disconnected chemical bonds increase exchange interactions, and as a result, increase polarization of the ions, while the relaxation of the atomic positions reduce exchange interactions and the polarizations. The atoms at the P-terminated (001) surface lose four of its nearest neighbors, but three nearest neighbors have been lost at the NaCs-terminated surface. As mentioned above, the relaxation affect the atomic positions at the NaCs-terminated slab more than P (As)-terminated one. Therefore, the observed increase in the polarization of the atoms at the P-terminated (001) surface could be related to the increase in exchange interactions due to the disconnection of the chemical bonds. The observed decline in the polarization of the atoms at the

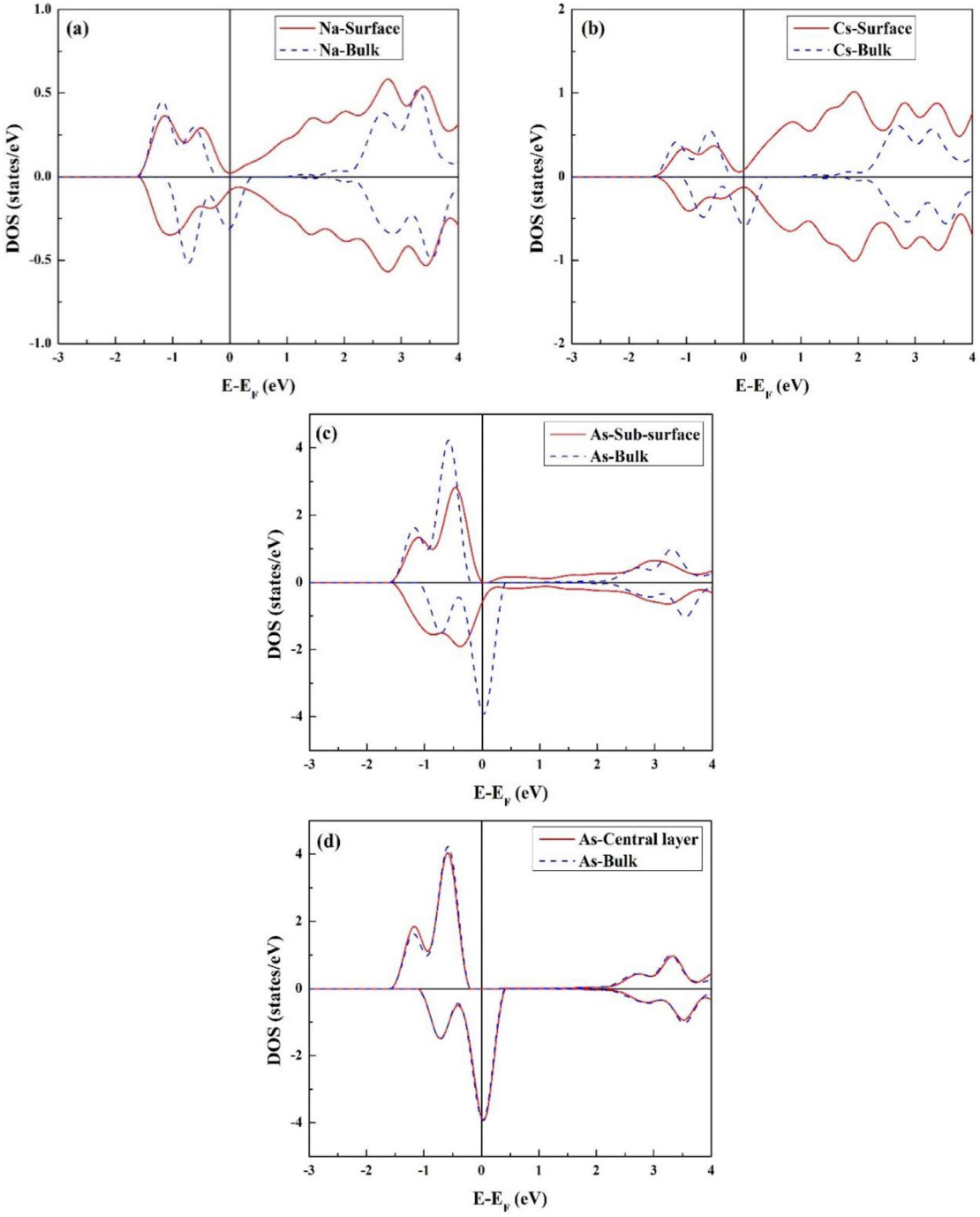

Fig. 12. The atomic density of states at various positions of the NaCs-terminated (001) slab of AsNaCs. The corresponding diagram for the bulk atoms are also given for analyzing.

NaCs-terminated (001) surface could also be due to the decrease in exchange interactions as a result of the changes in the positions caused by the relaxation of the atomic coordinates.

4. Conclusions

It is so advantageous to find half-metallic Heusler alloys without the transition elements as potential materials in spintronic devices because they could have low magnetic moments, high Curie temperatures and similar crystal structures to the semiconductors. Besides, an efficient half-metallic ferromagnet should preserve the half-metallicity at its surfaces to transfer the spin-polarized current to the other parts of the spintronic instruments. Therefore, the electronic and half-metallic properties of MNaCs (M = P and As) and the (001) surfaces of them were investigated, and the results of our calculations show that these compounds have all of the properties mentioned above. Both of these compounds are half-metallic ferromagnets with Spin-flip gaps of 0.25 and 0.21 eV, and the Curie temperatures are 478.24 and 474.07 K, respectively. It is found that the half-metallic ferromagnetism is due to the higher magnetic band splitting caused by the molecular field with respect to the width of the bands originated from P-p orbitals. Considering the band structures of the compounds under stress, we

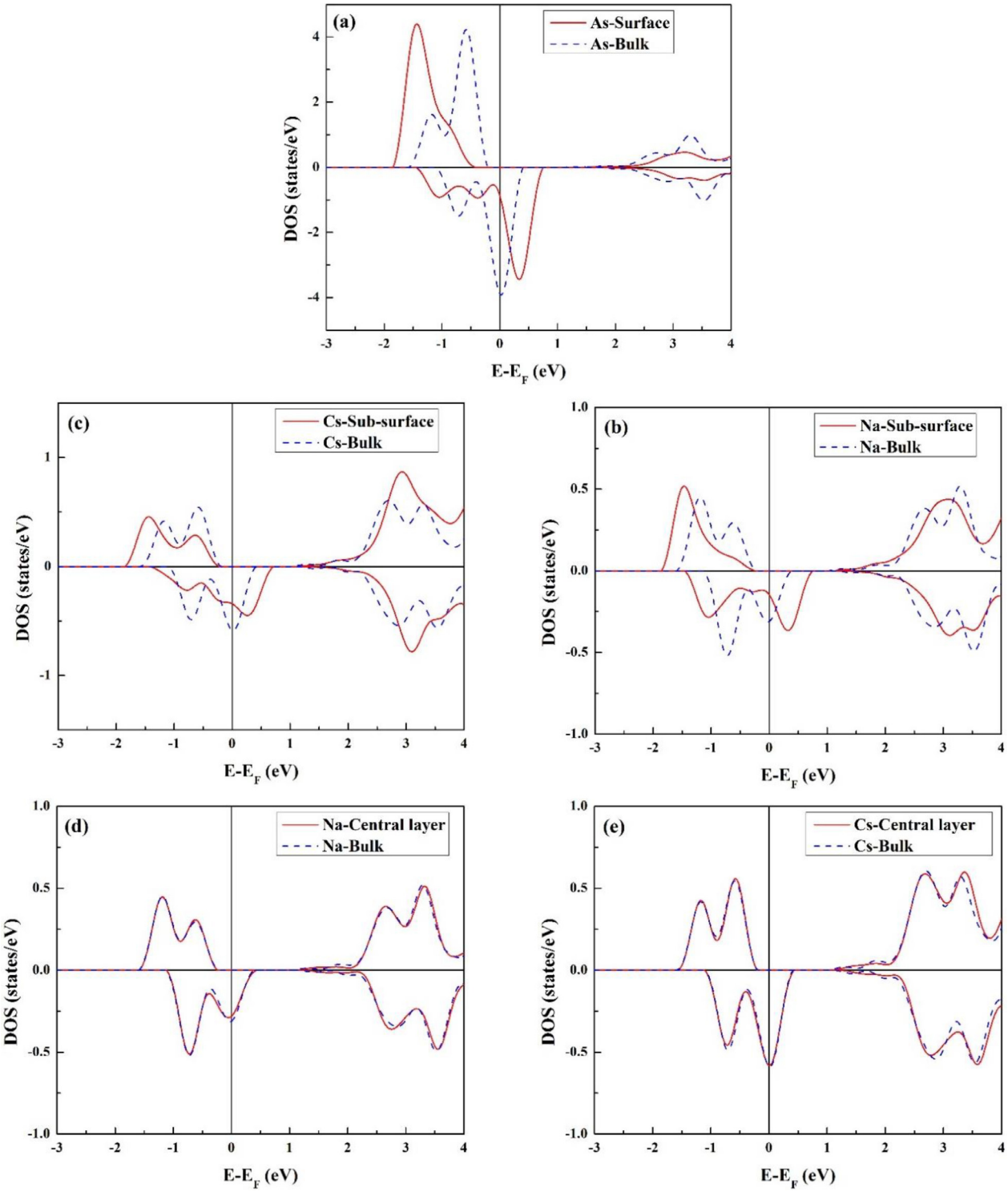

Fig. 13. The atomic density of states at various positions of the As-terminated (001) slab of AsNaCs. The corresponding diagram for the bulk atoms are also given for analyzing.

conclude that the half-metallicity is preserved for lattice compressions from −9.8% to +31.1%, and from −9.9% to +31.5% for PNaCs and AsNaCs, respectively. Symmetric slabs with the optimized number of eleven atomic layers and a vacuum thickness of 20 a.u. were used to investigate the electronic and half-metallic properties of (001) surfaces of PNaCs and AsNaCs. It is found that the decrease in exchange interactions as a result of changes in the atomic positions due to the relaxtion give rise to the removal of half-metallic ferromagnetism at the NaCs-terminated surfaces of both PNaCs and AsNaCs compounds. However, the bulk half-metallic property is well maintained at the P-terminated and As-terminated (001) surfaces. Therefore, it seems that MNaCs (M = P, As) half-Heusler compounds with the P (As)-terminated (001) surfaces are appropriate materials to be grown on semiconductors for various spintronic applications.

Table 4
The atomic magnetic moments at different positions of the NaCs-terminated and P-terminated (001) slabs of PNaCs and the corresponding bulk values.

Atom		NaCs-terminated	P-terminated	Bulk
P	Surface	–	1.6333	0.9682
	Sub-surface	0.0948	–	
	Central layer	1.0106	–	
Na	Surface	−0.0020	–	−0.0046
	Sub-surface	–	0.0622	
	Central layer	–	−0.0051	
Cs	Surface	−0.0165	–	0.0453
	Sub-surface	–	0.0928	
	Central layer	–	0.0494	

Table 5
The atomic magnetic moments at different positions of the NaCs-terminated and P-terminated (001) slabs of AsNaCs and the corresponding bulk values.

Atom		NaCs-terminated	As-terminated	Bulk
As	Surface	–	1.6300	0.9501
	Sub-surface	0.0873	–	
	Central layer	0.9942	–	
Na	Surface	−0.0024	–	0.0081
	Sub-surface	–	0.0772	
	Central layer	–	0.0066	
Cs	Surface	−0.0151	–	0.0610
	Sub-surface	–	0.1050	
	Central layer	–	0.0616	

Supplementary materials

Supplementary material associated with this article can be found, in the online version, at doi:10.1016/j.susc.2018.04.006.

References

[1] N.R. Checca, R.J. Caraballo-Vivas, R. Torrão, A. Rossi, M.S. Reis, Phase composition and growth mechanisms of half-metal Heusler alloy produced by pulsed laser deposition: from core-shell nanoparticles to amorphous randomic clusters, Mater. Chem. Phys. 196 (2017) 103–108.
[2] B. Balke, G. Fecher, C. Felser, New Heusler compounds and Their Properties, in: C. Felser, G.H. Fecher (Eds.), Springer, Berlin, 2013, pp. 15–43 Spintronic.
[3] Y.Z. Abdullahi, T.L. Yoon, M.M. Halim, M.R. Hashim, T.L. Lim, First-principles investigation of graphitic carbon nitride monolayer with embedded Fe atom, Surf. Sci. 667 (2018) 112–120.
[4] G. Torosyan, S. Keller, L. Scheuer, R. Beigang, E.T. Papaioannou, Optimized spintronic terahertz emitters based on epitaxial grown Fe/Pt layer structures, Sci. Rep. 8 (2018) 1311.
[5] K. Sato, L. Bergqvist, J. Kudrnovský, P.H. Dederichs, O. Eriksson, I. Turek, B. Sanyal, G. Bouzerar, H. Katayama-Yoshida, V.A. Dinh, T. Fukushima, H. Kizaki, R. Zeller, First-principles theory of dilute magnetic semiconductors, Rev. Mod. Phys. 82 (2010) 1633.
[6] R.A. Duine, K.-J. Lee, S.S.P. Parkin, M.D. Stiles, Synthetic antiferromagnetic spintronics, Nat. Phys. 14 (2018) 217–219.
[7] R. Mansell, D.C.M.C Petit, A. Fernández-Pacheco, R. Lavrijsen, J.H. Lee, R.P. Cowburn, Sputter grown Fe and Fe/Cr multilayers with fourfold magnetic anisotropy on GaAs, IEEE Trans. Magn. 54 (2018) 1–5.
[8] S.S.P. Parkin, M. Hayashi, L. Thomas, Magnetic domain-wall racetrack memory, Science 320 (2008) 190–194.
[9] A. Singh, C. Jansen, K. Lahabi, J. Aarts, High-quality CrO_2 nanowires for dissipation-less spintronic, Phys. Rev. X 6 (2016) 041012.
[10] M. Sun, X. Wang, W. Mi, Large magnetoresistance in Fe_3O_4/4,4′-bipyridine/Fe_3O_4 organic magnetic tunnel junctions, J. Phys. Chem. C 122 (2018) 3115–3122.
[11] G. Wang, Y. Liao, Theoretical prediction of robust and intrinsic half-metallicity in Ni_2N MXene with different types of surface terminations, Appl. Surf. Sci. 426 (2017) 804–811.
[12] A. Hirohata, H. Sukegawa, H. Yanagihara, I. Zutic, T. Seki, S. Mizukami, R. Swaminathan, Roadmap for emerging materials for spintronic device applications, IEEE Trans. Magn. 51 (2015) 1–11.
[13] G. Li, Y. Zhao, S. Zeng, J. Ni, The realization of half-metal and spin-semiconductor for metal adatoms on arsenene, Appl. Surf. Sci. 390 (2016) 60–67.
[14] Z.Y. Feng, J.M. Zhang, Structural, electronic, magnetic and optical properties of semiconductor $Zn_{1-x}Mo_xTe$ compound, J. Phys. Chem. Solids 114 (2018) 240–245.
[15] J.M.K Al-zyadi, N.H. Abdul-Wahhab, K.L. Yao, Half-metallicity of (001), (110) and (111) surfaces of zinc-blende MnBi and their interfaces with HgTe: a first-principle investigation, J. Magn. Magn. Mater. 446 (2018) 221–230.
[16] M. Kazemi, P. Amiri, H. Salehi, Density functional study of d0 half-metallic ferromagnetism in a bulk and (001) nano-surface of KP compound, Phys. Lett. A 381 (2017) 2420–2425.
[17] M. Rostami, M. Moradi, Electronic and magnetic properties of the bulk and surfaces of rocksalt KM (M = Se and Te): a density functional theory study, J. Supercond. Novel Magn. 29 (2016) 215–226.
[18] N. Mehmood, R. Ahmad, Structural, electronic, magnetic and optical investigations of half-Heusler compounds YZSb (Z = Cr, Mn): FP-LAPW method, J. Supercond. Novel Magn. 31 (2018) 879–888.
[19] M. Moradi, M. Rostami, M. Afshari, Half-metallic ferromagnetism in wurtzite and rocksalt TiTe: a density functional theory study, Comput. Mater. Sci. 69 (2013) 278–283.
[20] J. Zhang, W.J. Ji, J. Xu, X.Y. Geng, J. Zhou, Z.B. Gu, S.H. Yao, S.T. Zhang, Giant positive magnetoresistance in half-metallic double-perovskite Sr_2CrWO_6 thin films, Sci. Adv. 3 (2017) e1701473.
[21] B. Amin, F. Majid, M.B. Saddique, B.U. Haq, A. Laref, T.A. Alrebdi, M. Rashid, Physical properties of half-metallic $AMnO_3$ (A = Mg, Ca) oxides via ab initio calculations, Comput. Mater. Sci. 146 (2018) 248–254.
[22] S. Maqsood, M. Rashid, F.U. Din, M.B. Saddique, A. Laref, Theoretical investigation of half-metallic oxides $XFeO_3$ (X = Sr, Ba) via modified Becke–Johnson potential scheme, J. Electron. Mater. 47 (2018) 2032–2041.
[23] Z. Xu, Y. Li, Z. Liu, S.F. Liu, Electronic and magnetic behaviors of B, N, and 3d transition metal substitutions in germanium carbide monolayer, J. Magn. Magn. Mater. 451 (2018) 799–807.
[24] Y. Nie, M. Rahman, P. Liu, A. Sidike, Q. Xia, G. Guo, Room-temperature half-metallicity in monolayer honeycomb structures of group-V binary compounds with carrier doping, Phys. Rev. B 96 (2017) 075401.
[25] M. Ashton, D. Gluhovic, S.B. Sinnott, J. Guo, D.A. Stewart, R.G. Hennig, Two-dimensional intrinsic half-metals with large spin gaps, Nano Lett. 17 (2017) 5251–5257.
[26] J.J. He, Y.D. Guo, X.H. Yan, H.L. Zeng, Electronic, magnetic and transport properties of transition metal-doped holely C2N-h2D nanoribbons, Phys. B 528 (2018) 1–8.
[27] J.X. Wang, Z.B. Chen, Y.C. Gao, Phase stability, magnetic, electronic, half-metallic and mechanical properties of a new equiatomic quaternary Heusler compound ZrRhTiIn: a first-principles investigation, J. Phys. Chem. Solids 116 (2018) 72–78.
[28] R.K. Guo, G.D. Liu, T.T. Lin, W. Wang, L.Y. Wang, X.F. Dai, The electronic, structural and magnetic properties of Heusler compounds ZrCrCoZ (Z = B, Al, Ga, In): a first-principles study, Solid State Commun. 270 (2018) 111–118.
[29] K. Rajabi, F. Ahmadian, Half-metallicity in new Heusler alloys $NaTO_2$ (T = *Sc*, Ti, V, Cr, and Mn): a first-principles study, Solid State Commun. 271 (2018) 29–38.
[30] X. Wang, Z. Cheng, Y. Jin, Y. Wu, X. Dai, G. Liu, Magneto-electronic properties and tetragonal deformation of rare-earth-element-based quaternary Heusler half-metals: a first-principles prediction, J. Alloys Compd. 734 (2018) 329–341.
[31] S. Rezaei, F. Ahmadian, First-principles study of half-metallic properties in RbCaNZ (Z = O, S, and Se) quaternary Heusler compounds, J. Magn. Magn. Mater. 456 (2018) 78–86.
[32] Saleem. Yousuf, Dinesh.C. Gupta, Insight into half-metallicity, spin-polarization and mechanical properties of L21 structured MnY_2Z (Z = Al, Si, Ga, Ge, Sn, Sb) Heusler alloys, J. Alloys Compd. 735 (2018) 1245–1252.
[33] H.M. Huang, S.J. Luo, Y.C. Xiong, Pressure-induced electronic, magnetic, half-metallic, and mechanical properties of half-Heusler compound CoCrBi, J. Magn. Magn. Mater. 438 (2017) 5–11.
[34] A. Amudhavalli, R. Rajeswarapalanichamy, K. Iyakutti, Half metallic ferromagnetism in Ni based half Heusler alloys, Comput. Mater. Sci. 148 (2018) 87–103.
[35] N. Mehmood, R. Ahmad, Structural, electronic, magnetic, and optical properties of half-Heusler alloys RuMnZ (Z = P, As): a first-principle study, J. Supercond. Novel Magn. 31 (2018) 233–239.
[36] N. Mehmood, R. Ahmad, Structural, electronic, magnetic and optical investigations of half-Heusler compounds YZSb (Z = Cr, Mn): FP-LAPW method, J. Supercond. Novel Magn. 31 (2018) 879–888.
[37] M. Rostami, M. Moradi, Z. Javdani, H. Salehi, The electronic, magnetic and optical properties of Cr-doped MC (M = Si, Ge and Sn): a density functional theory approach, Mater. Sci. Semicond. Proc. 38 (2015) 218–227.
[38] D.E. Aimouch, S. Meskine, A. Boukortt, A. Zaoui, Effect of (Mn,Cr) co-doping on structural, electronic and magnetic properties of zinc oxide by first-principles studies, J. Magn. Magn. Mater. 451 (2018) 70–78.
[39] W. Akbar, S. Nazir, Origin of p-type half-metallic ferromagnetism in carbon-doped BeS: First-principles characterization, J. Alloys Compd. 743 (2018) 83–86.
[40] I.U.N. Lone, M.M.S. Sirajuddeen, Half metallic ferromagnetism in gallium and zinc doped chromium phosphide: first principles calculations, Mater. Chem. Phys. 203 (2018) 65–72.
[41] M. Rostami, M. Afshari, M. Moradi, Bulk and surface half-metallicity of CsS in CsCl structure: a density functional theory study, J. Alloys Compd. 575 (2013) 301–308.
[42] G.Y. Gao, K.L. Yao, M.H. Song, Z.L. Liu, Half-metallic ferromagnetism in rocksalt and zinc-blende MS (M = Li, Na and K): a first-principles study, J. Magn. Magn. Mater. 323 (2011) 2652–2657.
[43] A. Rath, C. Sivakumar, C. Sun, S.J. Patel, J.S. Jeong, J. Feng, G. Stecklein, P.A. Crowell, C.J. Palmstrøm, W.H. Butler, P.M. Voyles, Reduced interface spin polarization by antiferromagnetically coupled Mn segregated to the Co_2MnSi/GaAs (001) interface, Phys. Rev. B 97 (2018) 045304.
[44] S.D. Harrington, A.D. Rice, T.L. Brown-Heft, B. Bonef, A. Sharan, A.P. McFadden, J.A. Logan, M. Pendharkar, M.M. Feldman, O. Mercan, A.G. Petukhov, A. Janotti, L.C. Arslan, C.J. Palmstrøm, Growth, electrical, structural, and magnetic properties of half-Heusler $CoTi_{1-x}Fe_xSb$, Phys. Rev. Mater. 2 (2018) 014406.

[45] S.E Glover, T. Saerbeck, B. Kuerbanjiang, A. Ghasemi, D. Kepaptsoglou, Q. Ramasse, S. Yamada, K. Hamaya, T.P. Hase, V. Lazarov, G.R Bell, Magnetic and structural depth profiles of Heusler alloy $Co_2FeAl_{0.5}Si_{0.5}$ epitaxial films on Si (111), J. Phys. 30 (2018) 065801.
[46] B. Kuerbanjiang, C. Love, D. Kepaptsoglou, Z. Nedelkoski, S. Yamada, A. Ghasemi, Q.M. Ramasse, K. Hamaya, S.A. Cavill, V.K. Lazarov, Effect of annealing on the structure and magnetic properties of $Co_2FeAl_{0.5}Si_{0.5}$ thin films on Ge(111), J. Alloy. Compd. 748 (2018) 323–327.
[47] Y. Yang, Z.Y. Feng, J.M. Zhang, Surface thermodynamic stability, electronic and magnetic properties in various (001) surfaces of Zr_2CoSn Heusler alloy, Superlattices Microstruct. 117 (2018) 82–91.
[48] A.R. Chandra, V. Jain, N. Lakshmi, V.K. Jain, R. Jain, K. Venugopalan, Spin polarization in Co_2CrAl/GaAs 2D-slabs: a computational study, J. Magn. Magn. Mater. 448 (2018) 75–81.
[49] I. Di Marco, A. Held, S. Keshavarz, Y.O. Kvashnin, L. Chioncel, Half-metallicity and magnetism in the Co_2MnAl/CoMnVAl heterostructure, Phys. Rev. B 97 (2018) 035105.
[50] Y. Hu, J.M. Zhang, Thermodynamic stability, magnetism and half-metallicity of various (100) surfaces of Heusler alloy Ti_2FeSn, Mater. Chem. Phys. 192 (2017) 253–259.
[51] J.M.K. Al-zyadi, M.H. Jolan, K.L. Yao, Surface half-metallicity of half-Heusler compound FeCrSe and interface half-metallicity of FeCrSe/GaP, J. Magn. Magn. Mater. 403 (2016) 8–13.
[52] Y. Li, G.D. Liu, X.T. Wang, E.K. Liu, X.K. Xi, W.H. Wang, G.H. Wub, X.F. Dai, Half-metallicity of the bulk and (001) surface of NbFeCrAl and NbFeVGe Heusler compounds: a first-principles prediction, RSC Adv. 7 (50) (2017) 31707–31713.
[53] A.D. Becke, Perspective: fifty years of density-functional theory in chemical physics, J. Chem. Phys. 140 (18) (2014) 18A301.
[54] J.P. Perdew, K. Burke, M. Ernzerhof, Generalized gradient approximation made simple, Phys. Rev. Lett. 77 (1996) 3865–3868.
[55] P. Giannozzi, et al., QUANTUM ESPRESSO: a modular and open-source software project for quantum simulations of materials, J. Phys. 21 (2009) 395502.
[56] H.J. Monkhorst, J.D. Pack, Special points for Brillouin-zone integrations, Phys. Rev. B 13 (1976) 5188–5192.
[57] I. Galanakis, P. Mavropoulos, Zinc-blende compounds of transition elements with N, P, As, Sb, S, Se, and Te as half-metallic systems, Phys. Rev. B 67 (2003) 104417.
[58] M. Afshari, M. Moradi, M. Rostami, Structural, electronic and magnetic properties of the (001), (110) and (111) surfaces of rocksalt sodium sulfide: a first-principles study, J. Phys. Chem. Solids 76 (2015) 94–99.
[59] C.J. Palmstrøm, Heusler compounds and spintronics, Prog. Cryst. Growth Charact. Mater. 62 (2016) 371–397.
[60] Z. Nedelkoski, et al., Realisation of magnetically and atomically abrupt half-metal/semiconductor interface: $Co_2FeSi_{0.5}Al_{0.5}$/Ge(111), Sci. Rep. 6 (2016) 37282.
[61] Y. Fujita, M. Yamada, M. Tsukahara, T. Oka, S. Yamada, T. Kanashima, K. Sawano, K. Hamaya, Spin Transport and Relaxation up to 250K in heavily doped n-type Ge detected using $Co_2FeAl_{0.5}Si_{0.5}$ electrodes, Phys. Rev. Appl. 8 (1) (2017) 014007.
[62] F. Ahmadian, M.R. Abolhassani, S.J. Hashemifar, M. Elahi, Robust half-metallicity at the zinc-blende CrTe (001) surfaces and its interface with ZnTe (001), J. Magn. Magn. Mater. 322 (8) (2010) 1004–1014.